Quantum Dots Grown In-Situ by MOVPE: Sizes, Densities and Optical Properties

W. Seifert, N. Carlsson, P. Castrillo, D. Hessman,
J. Johansson, M-E. Pistol and L. Samuelson
Solid State Physics, Lund University,
Box 118, S-22100 Lund, Sweden
Fax: (-46 46) 2223637 E-mail: werner.seifert@ftf.lth.se

Received February 2, 1997

This paper focuses on the strain-induced self-organization, or "self- assembly" effect, producing quantum dots. Particularly the following aspects will be addressed: (i) the phenomenology of the 2D-3D morphology transition, (ii) the effects of materials choices and growth conditions on density, size and homogeneity of dots, (iii) manipulations to get laterally aligned and vertically stacked dot structures and (iv) optical properties of free-standing and buried dots of InP grown on GaInP/GaAs(001). Free-standing as well as buried dots of InP on GaInP/GaAs show luminescence and quantum confinement effects which depend on the size of the islands. Luminescence arising from single dots will be demonstrated.

I. Introduction

Low dimensional semiconductor structures have reached great interest due to their modified electronic and optical properties. Quantum dot structures, which provide electron confinement in three dimensions, can be grown in-situ, without using lithography, by the so called "self-assembly" effect or Stranski- Krastanow (SK) growth mode. In this growth mode at a certain critical thickness, an initially two-dimensional (2D) epitaxial layer under compressive strain relaxes into self organized three-dimensional (3D) coherent islands (dots), and a remaining thinner 2D wetting layer. By forming 3D islands the strain can relax in three dimensions and the total energy of the system is reduced.

Typical SK-systems investigated so far are islands formed by the materials $Si_{1-x}Ge_x$/Si [1], $Ga_{1-x}In_xAs$/GaAs [2,3l $Ga_{1-x}In_xAs$/AlGaAs [4], InP/GaInP [5-7], InP/GaAs [8], InAs/InP [9] and GaSb/GaAs [10]. Detailed studies about the island formation mechanism, mainly for the material combinations $Si_{1-x}Ge_x$/Si and InAs/GaAs have been done using molecular beam epitaxy (MBE) [3,11-16] as well as theoretical modeling [14,17-20]. Important parameters with the view of potential applications of such structures are the density and the size of the in-situ formed islands. Based on our experience in growing InP dot structures in a metal-organic vapour phase epitaxy (MOVPE) deposition system [7,21-23] we will show in the following that these parameters are to some degree determined by the deposition conditions. By this, also the dot-specific properties of these structures can be deliberately manipulated.

II. Phenomenology of the 2D-3D morphology transition

The *2D-3D transition is clearly driven by strain.* Therefore, the typical SK-systems are combinations of highly strained materials (with the epilayer under compression and a misfit of typically larger than 2-3 *release mechanism for the 2D-3D transition is a nucleation process,* following the general rules of nucleation and growth from a supersaturated mobile phase. A schematics of the process as discussed in ref. [23] is shown in Fig. 1. It shows qualitatively the changes in the total energy of a mismatched system vs. time. We assume that epilayer material (under compression) is deposited with a constant deposition rate until point X is reached. The plot can be divided into three sections:

period A (2D deposition), period B (2D-3D transition) and period C (ripening of islands).

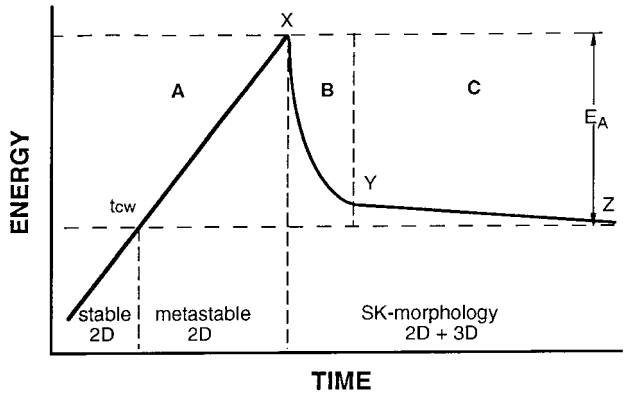

Figure 1. Schematics of total energy vs. time for the 2D-3D morphology transition. A: 2D layer-by-layer growth, B: 2D-3D-transition, C: ripening phase. t_{CW} is the critical wetting layer thickness, E_A is the barrier for formation of 3D islands, X is the point where a pure strain-induced transition becomes possible (no thermal activation). Between Y and Z a slow ripening process continues.

Period A: In the beginning the deposition follows a 2D layer-by-layer mechanism which leads to a perfect wetting of the substrate. The accumulated elastic strain energy E(el) increases linearly with the deposited volume:

$$E(el) = Cm^2At \qquad (1)$$

(with C: elastic coefficients, m: misfit, A: area and t: thickness of the epilayer). At the point t_{Cw} (the critical wetting layer thickness) we leave the stable 2D growth and enter into an area in which 2D growth is metastable. A supercritically thick wetting layer builds up, which means that the epilayer is potentially ready to undergo a transition towards a Stranski-Krastanow morphology. It is obvious that the extension of this range of metastability (and with it the amount of material which is available for 3D island growth) depends primarily on the height of the transition barrier E_A.

Period B: We presume that, if the 2D-3D transition starts around point X in Fig.1, then it continues without further materials supply, simply by consuming the excess material accumulated in the supercritically thick wetting layer. This period can be divided into two steps: nucleation and growth.

i) Nucleation: Exactly at point X a pure strain-induced 2D-3D transition becomes possible. However, at real growth temperatures an activated nucleation sets in before reaching X. The activation energy for this nucleation process is $E_A - E_E$ (with E_E: the excess energy in the metastable 2D layer). If we tentatively assume that thickness fluctuations lead to the formation of critical nuclei, then the classical nucleation theories predict for the simplest case [24]

$$dN/dt = const \;\; \sigma \;\; \exp[-(E_A - E_E)/kT] \qquad (2)$$

(with dN/dt: the number of critical nuclei created per time and σ: the "supersaturation", i.e., the concentration of mobile excess material at the surface). As soon as the first islands are created, E_E decreases due to more efficient strain relaxation within the 3D islands in comparison to the 2D layer and σ decreases since the islands start to grow and to consume the material which is available and mobile enough to reach the islands. The consequence is that nucleation is restricted to a short time-span in the beginning of the 2D-3D transition. Thus this nucleation step defines the surface density of the dots.

ii) Growth of islands: Due to the high supersaturation in the beginning of this period the islands are "pushed" to grow. The absolute growth rates can be extremely high. InP islands, for example, grow at 580^o in a few seconds (1-3s) up to 12-18 nm in [001] direction (compare the typical MOVPE growth rates in the order of 0.3 nm/s!). Since the growth rate on low-index facets in the kinetically controlled regime and also the diffusional transport towards the islands is strongly temperature- dependent, the islands grow faster at higher temperatures. Consequently, also the drop in supersaturation and the increase of the activation barrier for thermally activated nucleation is faster (eq.2). Fewer islands will be formed in the initial nucleation period and the excess material can be distributed over fewer islands which can then grow to larger sizes. This inverse behaviour of density and size is generally observed for islands of InP/GaInP [8], InAs/GaAs [25,26] and GaInAs/GaAs [27], see also our results below.

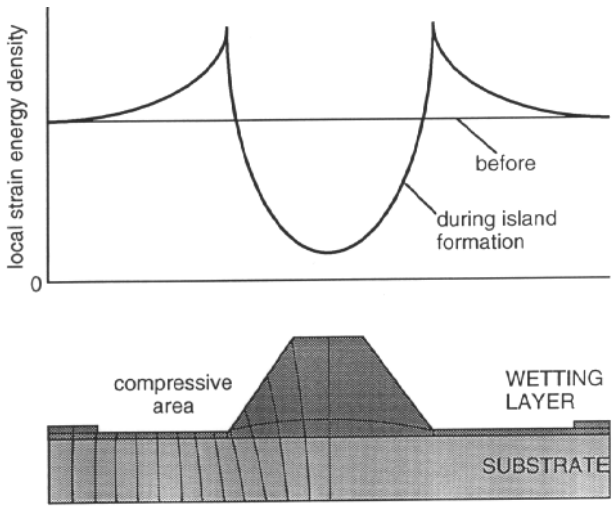

Figure 2. Schematics of deformation of lattice planes in and around a coherent island. The change in the local strain energy density at the surface when islands are formed is shown in the upper part of the Figure.

Another growth aspect is the rather high size-homogeneity of coherent SK dots. Fig.2 illustrates the strain energy density along the surface of substrate and island. This energy density is proportional to the chemical potential of the material at the surface. We see the surface of the island as the sink in this potential, whereas we find a maximum at the edge of the island. The minimum is caused by the partial strain relaxation in the islands and this is the driving force for material to crystallize at the islands surface. The maximum is caused by the high strain at the edge of the island [28,29] and its propagation along the substrate, which increases the inherent misfit between substrate and wetting layer material around the islands. This should be a driving force to decompose the material in this area, where the wetting layer was already supercritically thick before the islands were formed.

This strain field effects also the size-development. Since this potential surrounding the coherent islands increases with increasing island size (exactly with increasing aspect ratio), it acts simultaneously as a barrier for material transport towards the islands with the consequence that smaller islands will be favoured to grow faster than larger islands, thus narrowing the size-distribution (this is in contrast to the so-called "Ostwald-ripening").

Period C: Ripening. Between the points Y and Z in Fig.1 the process has lost most of the excess energy. The mobile material is consumed and the potential differences between slightly smaller and larger islands maintain a slow further reaction, mediated by surface diffusion, towards equilibrium (Ostwald ripening [24] or stable dot-arrays [14]).

III. Density, size and homogeneity of dots as a function of deposition parameters

III.1. Experiments

The following experiments were done under low-pressure MOVPE conditions (100 mbar) in a RF-heated reactor cell. Trimethylgallium (TMG), trimethylindium (TMI), PH_3, AsH_3 and GaAs (001)-substrates were used in H_2 as the carrier gas. The gas switchings were done by a flow- and pressure-balanced vent/run switching system. The switch from growth of GaAs toward growth of GaInP or InP was always done by inserting a thin (2ML) deposition of GaP [21]. Samples for AFM measurements were annealed for 12 s under PH_3 at deposition temperature before cooling down.

III.2. The different steps seen by photoluminescence (PL)

Fig.3 shows the development of 5K PL spectra of GaAs(001)/GaInP (300nm)/InP/GaInP(300nm) hetero-structures, grown at 580 ^{o}C and with different amounts of InP [7]. Up to 1.2 ML InP the deposition results in extended areas of 2D quantum wells, 1 and 2 ML thick, producing the sharp luminescence peaks at 1.95 and 1.92 eV. For 1.8 ML the quantum well luminescence broadens, indicating a roughening of the InP/GaInP interface. Finally, for 2.4 ML deposition a new luminescence with a doublet centered at 1.64 appears, which is characteristic for fully developed dots of InP, typically 45x60 nm at the base, 13 nm in height [30].

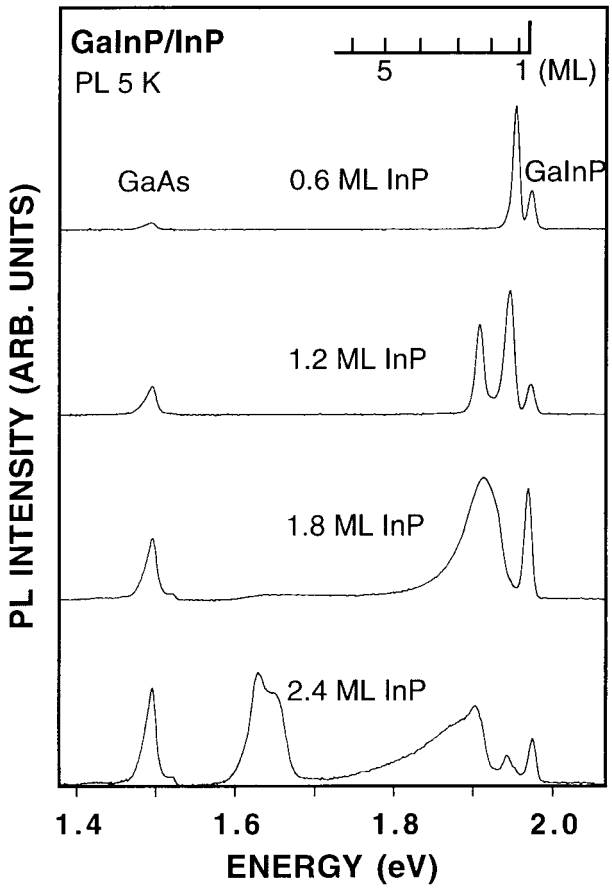

Figure 3. 5K Photoluminescence spectra of GaInP/InP/GaInP heterostructures with different amounts of InP (MOVPE, 580 °C). The peak at 1.5 eV originates from the GaAs substrate, the peak at 1.97 eV from the GaInP barrier. The insert shows calculated energy values for emission from biaxially strained InP quantum wells.

III. 3. Size and density of islands grown at different temperatures

These experiments were done by deposition of 2ML GaP + 3.5 ML InP on GaAs. Fig.4 shows the top-view AFM images. The density of the islands clearly decreases with increasing deposition temperature as a consequence of a shorter nucleation period due to faster materials diffusion and island growth. Due to the lower initial density of islands, the excess material distributes over fewer islands and, consequently, the size of the islands increases with temperature. The inverse behaviour of size and density is clearly visible in the graph of Fig.4.

In Fig. 4 is shown that an extrapolation towards lower temperatures roughly also fits to the observed size and density of islands of InAs on GaAs. The generally smaller size of InAs/GaAs islands in comparison to InP/GaAs islands, commonly attributed to the higher strain in the InAs/GaAs system, seems to be in first order an effect of growth at lower deposition temperatures.

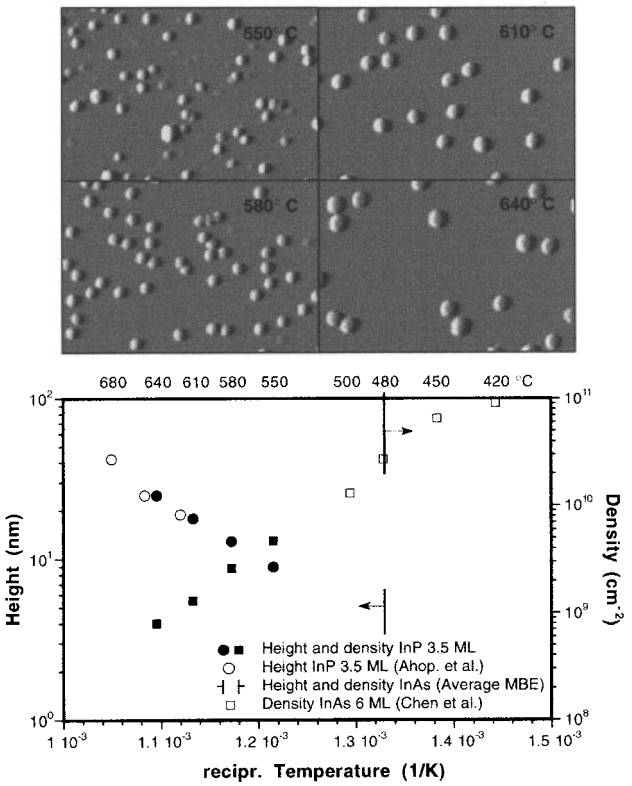

Figure 4. $1.5 \times 1\ \mu m^2$ AFM images (shadow mode) of InP dots grown on GaAs at different temperatures. The graph shows the height of the fully developed coherent islands (circles) and the surface density (squares) versus the reciprocal growth temperature. Open circles are taken from Ref. [8]. Deposited amount of InP: 3.5 ML.

III.4. Size and density of islands grown with different deposition rates

The AFM images of depositions of 2ML-GaP+3.5ML InP on GaAs are shown in Fig.5. The deposition rate was varied between 0.5 and 3.5 ML/s. The high uniformity of the islands size indicates that mainly coherent "fully developed" islands were grown. It can clearly be seen that the island density is decreasing for increasing temperature and decreasing deposition rate. Another effect is that the islands grown at higher temperatures are larger than the islands grown at lower temperature. These observations are in agreement with already reported results in the refs. [8,22,23,25,26,31-33]. This inverse behaviour between density and size of

the islands finds its natural explanation by using a simple kinetic model of nucleation and growth [22] where the nucleation step takes place during a short time period only in the beginning of the 2D-3D transition. The formation of 3D nuclei leads to strain relaxation and to a decrease of the strain potential as the driving force for the 2D-3D transition. The probability for further nucleation reduces drastically. Therefore, the amount of excess material at the surface, i.e. the material of the supercritically thick wetting layer plus impinging atoms due to deposition, will preferentially be incorporated into the already existing Islands. By this distribution of material it follows that the average island size has to increase for decreasing density, at the same coverage.

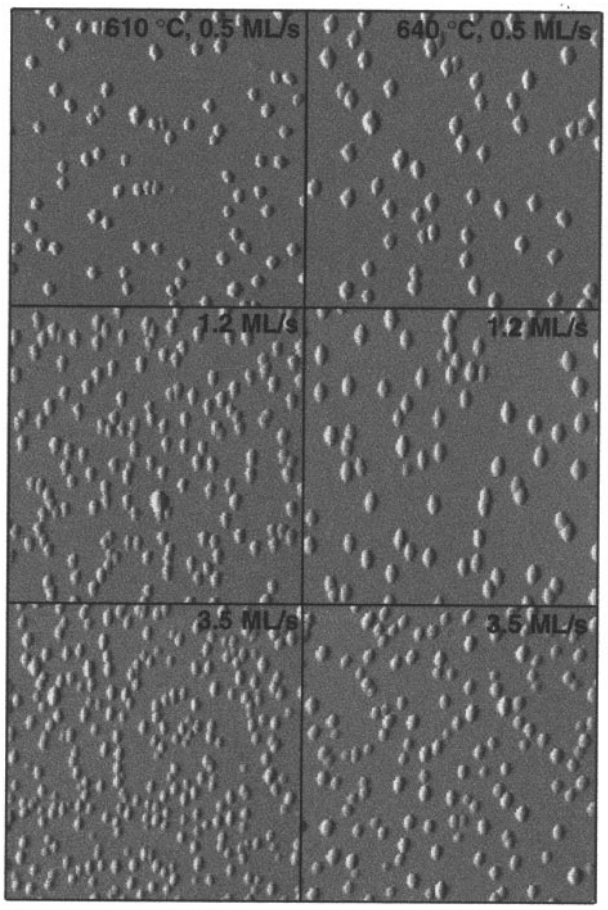

Figure 5. AFM images, 2×2 μm^2, of InP islands grown on GaAs. The temperature was 610 °C for a), b) and c), and 640 °C for d), e) and f). The deposition rates were 0.5 ML/s for a) and d), 1.2 ML/s for b) and e) and 3.5 ML/s for c) and f). The total amount of InP was 3.5 ML in all cases. All images are viewed in shadowed mode.

At this point it should be mentioned that the observed behaviour ls not a specifics of MOVPE growth. The characteristic length scale of surface processes is often written as $L \propto (D/R)^{\gamma}$, where the exponent γ is determined by the actual process. For sub-monolayer deposition γ varies between 1/6 and 1/4 [34]. For SK-growth γ is close to 1/2, as is shown by the slope of the line obtained for low values of R in Fig. 6. Other strained materials combinations show the same behaviour. See for instance InAs/GaAs [26] and SiGe/Si [33], both grown by MBE, which are included in Fig. 6.

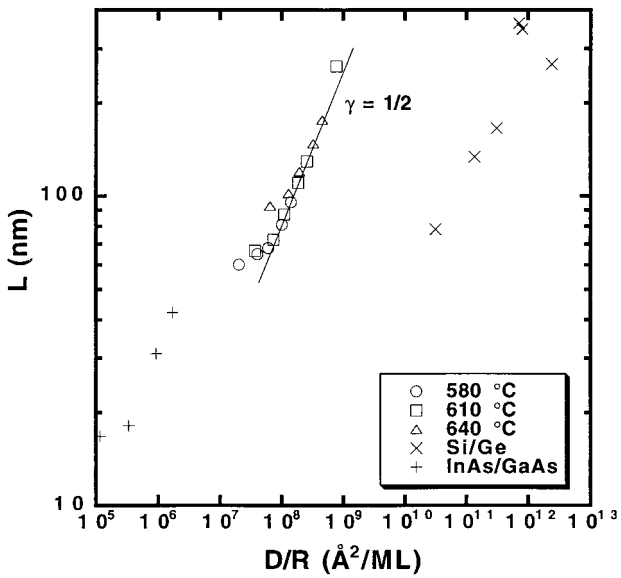

Figure 6. The average island separation, L as a function of D/R. The 580 °C, 610 °C and 640 °C curves account for InP islands on GaAs. These three curves tend to reach saturation values for L, related to the saturation densities, for sufficiently low D/R. The values for InAs/GaAs were extracted from ref. [26] and those for Si/Ge from ref. [33].

III.5. Towards positioning of dots

In order to overcome the randomness in the local distribution of dots one has the possibility to align them laterally or to stack them vertically. In both cases one needs a pattern of preferential nucleation sites. These pattern can be: single [11] or bunched [35] surface steps, etched pattern [36,37], pattern produced by overgrowth of metal structures [38] or in case of vertical stacking: patterned strain fields, produced in a first "seed"-layer of dots [2,39-41]. Fig.7 shows aligned InP dots grown on patterned GaAs/W/GaInP surfaces (MOVPE, 580 °C, W-stripes 100 nm in widths, overgrown by GaAs/GaInP [38]). At the moment the detailed mechanisms are not well understood. The dots in this case nucleate

in rows along the bottom of the trench as well as along the upper part of the side-wall. In similar structures with ridges instead of trenches the islands were found to nucleate in rows on top of the ridge. This alignment has also a concentration effect: when we count the islands, including the "vacancies", along the line b) in Fig.7, we come to an average of about 10 dots/,um, corresponding to a surface density of 10^{10} dots/cm^2 and an average distance of 100 nm between the dots. This distance is shorter than the average of about 200 nm observed for a random deposition of 4 ML InP. A way to bring the islands closer together is vertical stacking, where a first "seed"-layer of dots is overgrown by the barrier material. In subsequent depositions of islands the arrangement in the layer below may be reproduced. One can imagine that the combination of lateral alignment and vertical stacking opens a door for highly advanced materials engineering work on a nano-scale, using such dots as the building blocks.

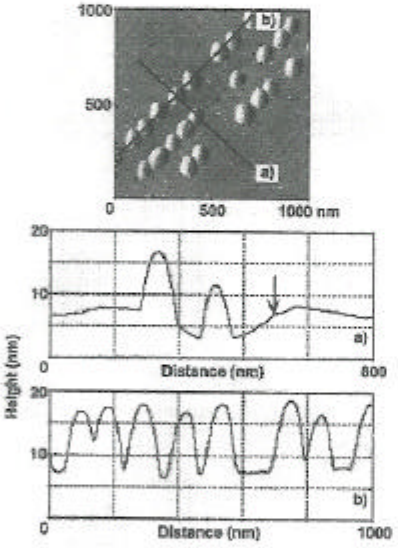

Figure 7. 1×1 μm^2 top-view AFM image (shadow mode) of aligned InP islands grown on a patterned GaAs/GaInP structure. a) Height profile across a trench. Note the location of the left island at the upper part of the sidewall. The arrow marks the position of a smaller "baby"-island in mirror position. b) Height profile along the island row at the edge of the trench. The linear 1D island density (by counting also the "vacancies") is $\approx$10 islands μm^{-1}.

IV. Optical properties of InP dots on GaInP/GaAs

InP islands have an important spectroscopic advantage since they emit light in a wavelength range where the most sensitive detectors work. TEM shows that the InP islands are truncated pyramids with a height of 12-15 nm and a base of 40 nm x 50 nm [30]. This makes the InP island an interesting low-dimensional system, being on the border between a QW and a quantum dot. Calculating the electronic structure in such a pyramid shaped quantum dot give fully quantised electron states, rather equidistantly spaced by some 10 meV. The hole states are, mainly due to the larger effective mass, only split by about 1 meV. Each island has several electron states, in contrast to the InAs islands in GaAs, allowing, for example, the study of interaction between localised carriers.

The PL corresponding to the islands is strongly nonlinear with excitation power densities above approximately 40 W/cm^2. The high- energy side of the PL peak grows rapidly all the way up to the GaInP barrier emission. In ref. [42] this is shown to be due to the successive filling of the states in the InP islands.

In usual PL experiments the PL signal is averaged over a large number of islands with slightly different properties, thus inducing an inhomogenous broadening of the spectral features. To observe details that are normally obscured by the inhomogenous broadening it is necessary to perform spectroscopy on a single InP island. The luminescence spectrum of a single zero-dimensional object with well separated, discrete energy states, is expected to consist of sharp lines, with a peak width determined by the life time broadening. In the InAs/GaAs S-K system, sharp lines are reported when less than some hundred islands are excited.

Single islands of InP on GaInP are selected by measuring through different 0.5 mm^2 holes in a gold mask. A PL spectrum obtained in such a hole is shown in Fig. 8 together with a normal PL spectrum. The luminescence between 1.6 eV and 1.7 eV in the micro-PL spectrum, originates from a single InP island. The most remarkable feature is that this single island gives rise to several luminescence peaks, as is more clearly shown in Fig. 9 [51]. The multiple emission lines of the InP island reveal that the relaxation within the set of states that give rise to the PL manifold is slower than the recombination rate. This is confirmed by PLE experiments, in which excitation energies within the energy range of the PL manifold gives very weak luminescence.

Excitation energies above the PL manifold, however, efficiently pump the luminescing states. The slow relaxation within the PL manifold is in contrast to the case of quantum wells which exhibit only a single emission line since relaxation by emission of phonons efficiently brings all carriers to the bottom of the lowest subband.

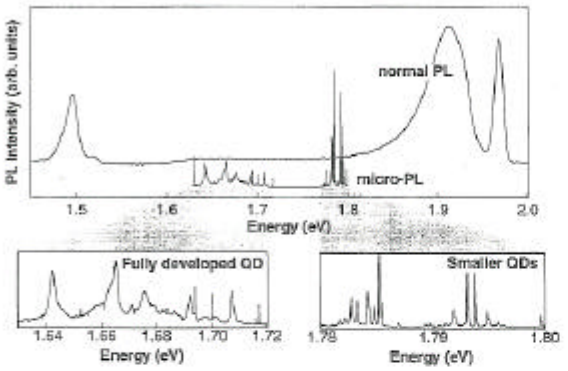

Figure 8. Comparison between ordinary PL and PL measured through a sub-micrometer sized hole in a gold mask (micro-PL).

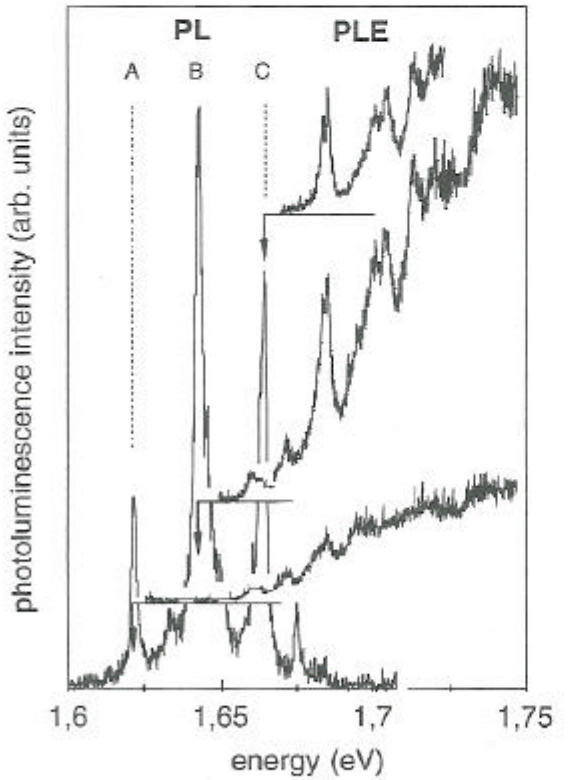

Figure 9. Emission spectrum of a single buried InP quantum dot. Also shown are the PL excitation spectra of of the peaks A, B and C, resp. [51].

A possible reason for the poor relaxation within the PL manifold of the InP islands is a phenomenon known as the phonon bottleneck [43,44], stating that neither optical nor acoustic phonon scattering is efficient in zero-dimensional systems. This subject, however, is still controversial [45]. Since the InP islands are rather large, the slow relaxation can also be explained if the non-relaxing states are localised in different regions of an island.

The state filling shows up in the single island as a population of discrete high energy peaks as the excitation density is increased. These 10 high energy peaks coincide in energy with resonances observed in PLE and they are therefore interpreted as excited states. Detecting on any peak in the PL manifold gives the same resonances in PLE, providing an important proof that one island give rise to all the emission in the PL manifold.

The line width of the peaks in the PL manifold is about 1 meV. This is significantly larger than the life time broadening, which, based on time- resolved PL, is expected to be 1 μeV. Line widths on the order of 1 meV have also been observed in other QD systems [46,47]. However, in the cases of InAs islands in GaAs [48] and excitons localised in potential fluctuations in a QW [49,50], much sharper PL lines are detected. Such sharp lines are found also in the present study. This is, for example, the case for the 1.79 eV emission in the micro-PL spectrum of figure 8. These sharp PL lines originate in smaller InP islands.

The main result of the single island spectroscopy is the slow relaxation rate, leading to multiple emission peaks, and the rather broad line width of about 1 meV. These findings still lack a satisfying explanation, in particular in view of the observations of single and/or sharp lines that has been reported from other quantum dot systems. It should be noted, however, that not many other spectroscopic studies on truly single islands have been done. Speculating, a general trend seems to be that small dots have sharp and, possibly, single emission lines while larger dots have broader and multiple [46] emission lines. In our InP islands, the emission, and thus also the reduced relaxation, is spread over about 50 meV (close to the 40 meV of an optical phonon). In a small dot with large enough confinement, however, there might be only one state available within

these 50 meV, thus resulting in a single emission line. The most probable cause of the line width broadening for the InP islands is a coupling between excitons and acoustic phonons via the piezo electric field. Due to the considerable amount of strain in the S-K islands, the piezo electric field is expected to be large. A line width broadening of 1 meV is thus not unlikely.

V. Summary

We have demonstrated that density and size of quantum dots grown in-situ by MOVPE can be manipulated to some degree by varying the deposition parameters. The generally observed inverse behaviour of density and size finds its natural explanation by using a simple model of nucleation and growth where the nucleation step takes place during a short time period only in the beginning of the 2D-3D transition. The control of the nucleation step for dot formation is therefore the main tool to define the dot parameters. By using appropriately patterned surfaces the dots can be positioned at special surface sites.

Photoluminescence measurements of single InP dots show multiple emission peaks due to a slow relaxation rate between the different states. It can be speculated whether this is a consequence of the "bottleneck"- effect.

References

1. D. J. Eaglesham and M. Cerullo, Phys. Rev. Lett. **64**, 1943 (1990).
2. L. Goldstein, F. Glas, J. Y. Marzin, M. N. Charasse and G. L. Roux, Appl. Phys. Lett. 47, 1099 (1985).
3. S. Guha, A. Madhukar and K. C. Rajkumar, Appl. Phys. Lett. **57**, 2110 (1990).
4. R. Nötzel, J. Temmyo, and T. Tamamura, Nature **369** 131 (1994).
5. S. P. DenBaars, C. M. Reaves, V. Bressler-Hill, S. Varma, H. Weinberg and P. M. Petroff, J. Crystal Growth **145**, 721 (1994).
6. J. Ahopelto, H. Lipsanen, M. Sopanen, Y. T. Koljonen and H. E. M. Niemi, Appl. Phys. Lett. **65**, 1662 (1994).
7. N. Carlsson, W. Seifert, A. Petersson, P. Castrillo, M.-E. Pistol and L. Samuelson, Appl. Phys. Lett. **65**, 3093 (1994).
8. M. Sopanen, H. Lipsanen and J. Ahopelto, Appl. Phys. Lett. **67**, 3768 (1995).
9. A. Ponchet, A. L. Corre, H. L'Haridon, B. Lambert and S. Salaun, Appl. Phys. Lett. **67**, 1850 (1995).
10. F. Hatami, N. N. Ledentsov, M. Grundmann, J. Bohrer, F. Heinrichsdorff, M. Beer, D. Bimberg, S. Ruvimov, P. Werner, U. Gosele, J. Heydenreich, U. Richter, S. V. Ivanov, B. Y. Meltser, P. S. Kop'ev and Z. I. Alferov, Appl. Phys. Lett. **67**. 656 (1995).
11. D. Leonard, K. Pond and P. M. Petroff, Phys. Rev. B **50**, 11687 (1994).
12. J. M. Moison, F. Houzay, F. Barthe, L. .Leprince, E. Andre and O. Vatel, Appl. Phys. Lett. **64**, 196 (1994).
13. Y. Nabetani, T. Ishikawa, S. Noda and A. Akasaki, J. Appl. Phys. **76**, 347 (1994).
14. V. A. Shchukin, N. N. Ledentsov, P. S. Kop'ev and D. Bimberg, Phys. Rev. Lett. **75**, 2968 (1995).
15. J.-M. Gerard, in *Confined Electrons and Photons*, Series B340 ed., edited by E. Burstein, C. Weisbuch (Plenum Press, New York, 1995), p. 357.
16. J. M. Gerard, J. B. Genin, J. Lefebvre, J. M. Moison, N. Lebouche and F. Barthe, J. Crystal Growth **150**, 351 (1995).
17. C. Ratsch and A. Zangwill, Surf. Sci. **293** 123 (1993). .
18. B. G. Orr, D. Kessler, C. W. Snyder and L. Sander, Europhys. Lett. **19**, 33 (1992).
19. C. Priester and M. Lannoo, Phys. Rev. Lett. **75**, 93 (1995).
20. P. Müller and R. Kern, JCG?preprint (1995).
21. N. Carlsson, K. Georgsson, L. Montelius, L. Samuelson, W. Seifert and R. Wallenberg, J. Crystal Growth **156**, 23 (1995).
22. W. Seifert, N. Carlsson, J. Johansson, M.-E. Pistol and L. Samuelson, J. Crystal Growth submitted (1996) .
23. W. Seifert, N. Carlsson, M. Miller, M.-E. Pistol, L. Samuelson and L. R. Wallenberg, Prog. Crystal Growth and Charact. **33**, 423 (1996).
24. M. Zinke-Allmang, L. C. Feldman and M. H. Grabow, Surf. Sci. Reports **16**, 377-463 (1992).

25. G. S. Solomon, J. A. Trezza and J.S. Harris, Jr., Appl. Phys. Lett. **66**, 991 (1995).
26. P. Chen, Q. Xie, A. Madhukar, L. Chen and A. Konkar, J. Vac. Sci. Technol. **B12**, 2568 (1994).
27. J. Oshinowo, M. Nishioka, S. Ishida and Y. Arakawa, Appl. Phys. Lett. **65**, 1421 (1994).
28. M. Berti, A. V. Drigo, A. Giuliani, M. Mazzer, A. Camporese, G. Rossetto and G. Torzo, J. Appl. Phys. **80**, 1931 (1996).
29. Y. Chen and J. Washburn, Phys. Rev. Lett. **77**, 4046 (1996).
30. K. Georgsson, N. Carlsson, L. Samuelson, W. Seifert and L. R. Wallenberg, Appl. Phys. Lett. **67**, 2981 (1995).
31. G. S. Solomon, J. A. Trezza and J.S. Harris, Jr., Appl. Phys. Lett. **66**, 3161 (1995).
32. R. E. Welser and L. J. Guido, Appl. Phys. Lett. **68**, 912 (1996).
33. G. Abstreiter, P. Schittenhelm, C. Engel, E. Silveira and A. Zrenner, Semicond. Sci. Technol. **11**, 1521 (1996).
34. S. V. Ghaisas and S. D. Sarma, Phys. Rev. B **46**, 7308 (1992).
35. M. Kitamura, M. Nishioka, J. Oshinowo and Y. Arakawa, Appl. Phys. Lett. **66**, 3663 (1995).
36. D. S. L. Mui, D. Leonard, L. A. Coldren and P. M. Petroff, Appl. Phys. Lett. **66**, 1620 (1995).
37. S. Jeppesen, M. Miller, D. Hessman, B. Kowalski, I. Maximov and L. Samuelson, Appl. Phys. Lett. **68**, 2228 (1996).
38. W. Seifert, N. Carlsson, A. Petersson, L.-E. Wernersson and L. Samuelson, Appl. Phys. Lett. **68**, 1684 (1996).
39. Q. Xie, A. Madhukar, P. Chen, and N. P. Kobayashi, Phys. Rev. Lett. **75**, 2542 (1995).
40. G. S. Solomon, J. A. Trezza, A. F. Marshall and J. S. Harris, Jr., Phys. Rev. Lett. **76**, 952 (1996).
41. M. S. Miller, J. O. Malm, M.-E. Pistol, S. Jeppesen, B. Kowalski, K. Georgsson and L. Samuelson, J. Appl. Phys. **80**, 3360 (1996).
42. P. Castrillo, D. Hessman, M.-E. Pistol, S. Anand, N. Carlsson, W. Seifert and L. Samuelson, Appl. Phys. Lett. **67**, 1905 (1995).
43. U. Bockelmann and G. Bastard, Phys. Rev. B **42**, 8947 (1990).
44. H. Benisty, C. M. Sotomayor-Torres and C. Weisbuch, Phys. Rev. B **44**, 10945 (1991).
45. Y. Arakawa, in *23rd Int. Conf. on the Physics of Semiconductors*, Berlin, 1996.
46. K. Brunner, U. Bockelmann, G. Abstreiter, M. Walther, G. Bohm, G. Trankle and G. Weimann, Phys. Rev. Lett. **69**, 3216 (1992).
47. Y. Nagamune, H. Watabe, M. Nishioka and Y. Arakawa, Appl. Phys. Lett. **67**, 3257 (1995).
48. J.-Y. Marzin, J.-M. Gerard, A. Izrael and D. Barrier, Phys. Rev. Lett. **73**, 716 (1994).
49. K. Brunner, G. Abstreiter, G. Bohm, G. Trankle and G. Weimann, Appl. Phys. Lett. **64**, 3320 (1994).
50. D. Gammon, E. S. Snow and D. S. Katzer, Appl. Phys. Lett. **67**, 2391 (1995).
51. D. Hessman, P. Castrillo, M.-E. Pistol, C. Prior and L. Samuelson, Appl. Phys. Lett. **69**, 749 (1996).